AIMS Mathematics, 10(3): 5332–5352.
DOI: 10.3934/math.2025246
Received: 06 January 2025
Revised: 18 February 2025
Accepted: 19 February 2025
Published: 10 March 2025

https://www.aimspress.com/journal/Math

Research article

Advancing water quality management: A synergistic approach using fractional differential equations and neural networks

Ateq Alsaadi *

Department of Mathematics and Statistics, College of Science, Taif University, P.O. Box 11099, Taif 21944, Saudi Arabia

* **Correspondence:** Email: ateq@tu.edu.sa.

Abstract: Water pollution significantly threatens public health and environmental sustainability, particularly in developing nations. This study introduced an innovative fractional-order mathematical model for analyzing water pollution dynamics, incorporating four distinct compartments to represent the interactions between polluted water sources, susceptible water bodies, contamination processes, and restoration mechanisms. The model used the Atangana-Baleanu fractional derivative in the Caputo sense, offering a more precise representation of memory effects and complex pollutant transport mechanisms. The proposed model underwent rigorous qualitative validation, ensuring the existence and uniqueness of solutions via fixed-point theory, while stability analysis was conducted using the Ulam-Hyers approach. The Adams-Bashforth numerical method was employed to obtain approximate solutions, enabling a more accurate simulation of pollution dynamics. Numerical simulations further highlighted the impact of treatment strategies in reducing contamination levels and restoring water quality. Additionally, artificial neural networks (ANN) were integrated into the framework to enhance predictive capabilities. The dataset used for ANN training was derived from simulated pollution levels based on model parameters calibrated with empirical studies on water contamination dynamics. This combined fractional-ANN methodology established a robust foundation for effective water quality management, aiding in decision-making for pollution control policies and remediation strategies.

Keywords: water quality management; mathematical modeling; fractional derivatives; qualitative analysis; ABC fractional derivative; stability analysis; numerical simulation; Adam–Bashforth method
Mathematics Subject Classification: 34D20, 34K20, 34K60, 92C60, 92D45

1. Introduction

Water pollution poses a significant challenge to global sustainability, disproportionately affecting developing nations. The adverse impacts on ecosystems, public health, and economic stability are

profound, with polluted water serving as a carrier for numerous waterborne diseases such as cholera, typhoid, diarrhea, hepatitis, and schistosomiasis [1]. In regions with limited access to clean water and healthcare, these illnesses can escalate into severe public health crises. Additionally, chronic exposure to contaminated water, laden with heavy metals and chemical pollutants, increases risks of cancer, neurological disorders, and cardiovascular diseases [2, 3]. Moreover, polluted aquatic ecosystems experience biodiversity loss, disrupting ecological balance and threatening livelihoods dependent on fishing and agriculture [4].

Mathematical modeling is indispensable in analyzing water pollution dynamics and mitigation strategies. Models provide insights into pollutant transport mechanisms, interaction with environmental variables, and spatial-temporal behaviors. For example, Guo and Cheng [5] demonstrated pollutant dispersion in Yuncheng City, China, revealing a reduction in concentration downstream, while Issakhov et al. [6] emphasized temperature's role in industrial chemical reactions through numerical simulations. Similarly, integrating computational models with real-world data has been pivotal in advancing our understanding of pollutant dynamics.

Fractional calculus has got much attention from the researchers nowadays because of their application in real world problems. In the realm of this area, Riemann-Livilave explored some basics for mathematical models. Caputo has done significance work and documented a derivative for fractional order, and after that, numerous work has been added in the literature of fractional calculus [7, 8]. After this approach, Caputo and Fabrizio further modified this definition into non-singular kernels and named it Caputo-Fabrizio (CF) [9]. Multiple works have been documented by applying the CF operator to the mathematical disease model and other complex models in the field of mathematics [10–12]. In 2016, Atangana and Baleanu generalized the CF derivative into non-singular and nonlocal kernels with a tremendous application in disease mathematical modeling, which is considered a new window for the researchers [13]. They called this new operator Atangana-Baleanu in the sense of Caputo (ABC) and this filled the gap of the previously mentioned operator. Many scholars have applied this new operator to real-world linear and nonlinear mathematical models and explored its different characteristics for the readers [14–17].

Recent advancements in fractional modeling offer improved accuracy in representing water pollution phenomena. With its ability to model memory effects and complex interactions, fractional calculus has been employed by Sabir et al. [18] to predict pollution behavior using the Levenberg-Marquardt backpropagation method. Artificial intelligent and machine learning have been a tremendous approach to mathematical problems. Recent advances in fractional calculus have demonstrated its effectiveness in various dynamic systems, including tumor-immune surveillance models [19], human infection modeling using real-world epidemiological data [20–23] and water pollution management with optimal control strategies [24]. These studies highlight the potential of fractional-order models in capturing long-term dependencies and improving predictive accuracy in environmental systems. Inspired by this, our study employs the Atangana-Baleanu fractional derivative to develop a robust mathematical framework for analyzing water contamination dynamics, integrating fractional differential equations with artificial neural networks (ANNs) for enhanced predictive modeling. Additionally, integrating ANN with fractional differential equations provides a hybrid predictive framework, making it more adaptable than purely empirical ANN-based pollution models. This combined approach enhances stability, long-term prediction accuracy, and computational efficiency compared to existing techniques. The concept of dynamical analysis in a

discrete-time SIR epidemic model was used in [25]. Ebrahimzadeh et al. [24] proposed a fractional framework combined with optimal control, showcasing its efficacy in water quality management. Remote sensing and machine learning techniques have further enhanced monitoring capabilities, as demonstrated by Chen et al. [2], enabling real-time assessments of water pollution [1].

Despite these advancements, existing models often face challenges in capturing water pollution's multifaceted and nonlinear nature. Complex interactions between pollutants, biological systems, and environmental variables require robust frameworks integrating computational, mathematical, and experimental approaches [4, 26]. Additionally, addressing the impacts of climate change, urbanization, and industrialization on water systems remains an ongoing research priority. Advancements in machine learning, coupled with fractional modeling, offer promising directions for the future. Ultimately, the integration of advanced modeling techniques, stakeholder collaboration, and data-driven decision-making holds the potential to revolutionize water pollution management. Continued interdisciplinary efforts are crucial for developing adaptive, scalable, and sustainable solutions that safeguard global water resources, public health, and ecosystems.

Model formulation

Among the various fractional derivatives available in the literature, the ABC derivative was selected for the reconsidered model [27] used for this study due to these reasons: (i) for constant functions, the ABC derivative yields the same result as an integer-order differential equation, ensuring consistency with classical calculus; (ii) it allows the use of initial conditions in a format similar to standard differential equations, making it suitable for practical applications; and (iii) its computation involves solving an ordinary differential equation followed by applying a fractional integral to achieve the desired fractional order.

This section delves into the analysis of the proposed model:

$$\begin{aligned}
&{}^{ABC}\mathbf{D}^{\varsigma}_{\mathfrak{I}} W(\mathfrak{I}) = \Lambda - \alpha_1 W(\mathfrak{I}) S(\mathfrak{I}) - \alpha_2 W(\mathfrak{I}) I_p(\mathfrak{I}) + \rho\alpha_2 I_p(\mathfrak{I}) - \mu W(\mathfrak{I}),\\
&{}^{ABC}\mathbf{D}^{\varsigma}_{\mathfrak{I}} S(\mathfrak{I}) = \alpha_1 W(\mathfrak{I}) S(\mathfrak{I}) + \delta I_p(\mathfrak{I}) - (\theta_1 + \mu) S(\mathfrak{I}),\\
&{}^{ABC}\mathbf{D}^{\varsigma}_{\mathfrak{I}} I_p(\mathfrak{I}) = \alpha_2 W(\mathfrak{I}) I_p(\mathfrak{I}) - \rho\alpha_2 I_p(\mathfrak{I}) - (\delta + \theta_2 + \mu) I_p(\mathfrak{I}),\\
&{}^{ABC}\mathbf{D}^{\varsigma}_{\mathfrak{I}} N(\mathfrak{I}) = \theta_1 S(\mathfrak{I}) + \theta_2 I_p(\mathfrak{I}) - \mu N(\mathfrak{I}),\\
&W(0) = W_0, S(0) = S_0, I_p(0) = I_{p0}, N(0) = N_0.
\end{aligned} \tag{1.1}$$

The fractional model presented in (1.1) is organized into four categories: $W(\mathfrak{I})$, which represents the number of polluted water sources; $S(\mathfrak{I})$, indicating water sources prone to pollution; $I_p(\mathfrak{I})$, representing water sources contaminated by pollutants; and $N(\mathfrak{I})$, describing water sources restored from insoluble pollution through treatment processes. It simplifies contaminant behavior into soluble and insoluble categories with fixed transport rates. Seasonal fluctuations, industrial discharge variations, and external environmental factors are not explicitly incorporated, making this framework a foundational approach for future extensions. The parameters associated with the model are defined in the following Table 1.

Table 1. Parameters with details used in the model 1.1.

Notation	Details
Λ	Rate of water pollution
α_1	Transport rate for soluble water contaminants
α_2	Transport rate for insoluble water contaminants
ρ	Conversion rate of insoluble pollutants into water pollution
μ	Rate of removal of water pollutants
δ	Rate of conversion of insoluble pollutants into solutes
θ_1	Maximum capacity for treating soluble water pollutants
θ_2	Maximum capacity for treating insoluble water pollutants

This work explores a fractional model of water pollution management by incorporating four compartments by employing the ABC operator. The analysis confirms the existence results and the uniqueness of solution with the help of fixed point approach. Furthermore, the Ulam–Hyers (UH) concept is utilized to demonstrate the stability of the solution. Additionally, the Newton interpolation method is applied for deriving the approximate solutions of the aforementioned model by integrating a fractional parameter to enhance flexibility in numerical simulations across the four compartments. This approach facilitates a continuous spectrum, representing densities within the range [0,1]. The ABC derivative effectively models system dynamics, offering distinct advantages over classical and other fractional derivatives. Its non-singular and nonlocal kernel enables a more precise depiction of memory effects and long-range interactions, essential for capturing the intricacies of complex dynamic systems. Unlike traditional derivatives, the ABC operator eliminates singularities and locality constraints, providing a robust and realistic framework for analyzing dynamic behavior. The application of this operator improves numerical stability and accuracy, as evidenced by the faster convergence and enhanced stability observed in fractional-order systems simulated using the Adams-Bashforth (AB) iterative method. By overcoming the limitations of classical approaches, the ABC derivative has emerged as a foundational tool for modeling, analyzing, and simulating nonlinear and dynamic systems with greater precision and reliability.

The manuscript structure is as follows: Section 2 presents a summary of key definitions and symbols from fractional calculus. Section 3 provides a theoretical analysis of the model using fixed point theory and evaluates UH stability under minor variations in the initial conditions. Section 4 employs the AB method, a widely recognized approach, to obtain approximate solutions for the proposed model. Additionally, the numerical results are summarized. Additionally, we summarize the numerical simulation results using MATLAB 16 to visualize the outcomes. Finally, Section 5 concludes the study and highlights key findings.

2. Basic results

Fractional derivatives, particularly the ABC operator, have been widely used in environmental modeling due to their ability to capture memory effects and complex system interactions [7, 13]. Similarly, the Mittag-Leffler (ML) function is crucial in fractional differential equations, offering solutions with non-exponential decay behavior that better represent real-world phenomena [8].

Definition 2.1. Let $\mathbf{U}(\mathfrak{I}) \in \varsigma \in [0, 1]$. The fractional derivative in the Caputo sense with the ABC

operator is given by:

$$^{ABC}\mathbf{D}_{\mathfrak{I}}^{\varsigma}(\mathbf{U}(\mathfrak{I})) = \frac{M(\varsigma)}{1-\varsigma}\int_0^{\mathfrak{I}} \mathbf{E}_{\varsigma}\Big[\frac{-\varsigma}{1-\varsigma}(\mathfrak{I}-u)^{\varsigma}\Big]\frac{d}{du}\mathbf{U}(u)\,du, \tag{2.1}$$

where $M(\varsigma)$ is a normalization function satisfying $M(0) = M(1) = 1$, and $\mathbf{E}_{\varsigma}$ denotes the ML function, which is expressed as:

$$\mathbf{E}_{\varsigma}(y) = \sum_{k=0}^{\infty}\frac{y^k}{\Gamma(\varsigma k+1)}.$$

Definition 2.2. For $\mathbf{U}(\mathfrak{I}) \in L^1(0,T)$, the ABC fractional integral is expressed as:

$$^{ABC}\mathbf{I}_{\mathfrak{I}}^{\varsigma}\mathbf{U}(\mathfrak{I}) = \frac{1-\varsigma}{M(\varsigma)}\mathbf{U}(\mathfrak{I}) + \frac{\varsigma}{M(\varsigma)}\frac{1}{\Gamma(\varsigma)}\int_0^{\mathfrak{I}}(\mathfrak{I}-u)^{\varsigma-1}\mathbf{U}(u)\,du, \quad \mathfrak{I} > 0. \tag{2.2}$$

Lemma 2.1. *The solution to the given fractional differential equation for* $\varsigma \in (0,1]$ *satisfies:*

$$^{ABC}\mathbf{D}_{\mathfrak{I}}^{\varsigma}\mathbf{U}(\mathfrak{I}) = \mathbf{U}(\mathfrak{I}),$$
$$\mathbf{U}(\mathfrak{I}) = \mathbf{U}_0,$$

with the condition:

$$\mathbf{U}(\mathfrak{I}) = \mathbf{U}_0 + \frac{1-\varsigma}{M(\varsigma)}\mathbf{U}(\mathfrak{I}) + \frac{\varsigma}{M(\varsigma)}\frac{1}{\Gamma(\varsigma)}\int_0^{\mathfrak{I}}(\mathfrak{I}-u)^{\varsigma-1}\mathbf{U}(u)\,du. \tag{2.3}$$

3. Existence theory

This section evaluates the proposed model's practicality within real-world scenarios. Additionally, it provides results concerning the stability and existence of the solution to the problem under consideration. Consequently, the problem is reformulated as follows:

$$\begin{cases} ^{ABC}\mathbf{D}_{\mathfrak{I}}^{\varsigma}W(\mathfrak{I}) &= \mathbf{G}_1(W,S,I_p,N), \\ ^{ABC}\mathbf{D}_{\mathfrak{I}}^{\varsigma}S(\mathfrak{I}) &= \mathbf{G}_2(W,S,I_p,N), \\ ^{ABC}\mathbf{D}_{\mathfrak{I}}^{\varsigma}I_p(\mathfrak{I}) &= \mathbf{G}_3(W,S,I_p,N), \\ ^{ABC}\mathbf{D}_{\mathfrak{I}}^{\varsigma}N(\mathfrak{I}) &= \mathbf{G}_4(W,S,I_p,N). \end{cases} \tag{3.1}$$

Writing Eq (1.1) in the form

$$^{ABC}\mathbf{D}_{\mathfrak{I}}^{\varsigma}\mathbf{U}(\mathfrak{I}) = \eta(\mathfrak{I},\mathbf{U}(\mathfrak{I})),$$
$$\mathbf{U}(0) = \mathbf{U}_0(\mathfrak{I}), \tag{3.2}$$

where

$$\begin{cases} \mathbf{U}(\mathfrak{I}) := (W,S,I_p,N)^T, \\ \mathbf{U}_0 := (W_0,S_0,I_{p_0},N_0)^T, \\ \eta(\mathfrak{I},\mathbf{U}(\mathfrak{I})) := \mathbf{G}_i(W,S,I_p,N)^T, \quad i = 1,2,3,4, \end{cases} \tag{3.3}$$

where $(.)^T$ denotes the transpose of the vector. The integral equation derived from system (3.2) can be expressed as:

$$\mathbf{U}(\mathfrak{I}) = \mathbf{U}_0 + \frac{1-\varsigma}{M(\varsigma)} Z(\mathfrak{I}, \mathbf{U}(\mathfrak{I})) + \frac{h}{M(\varsigma)\Gamma(\varsigma)} \int_0^{\mathfrak{I}} (\mathfrak{I}-\varphi)^{\varsigma-1} Z(\varphi, \mathbf{U}(\varphi)) d\varphi. \tag{3.4}$$

Consider the Banach space $\Upsilon = C([0,T], \mathbf{R}^k)_{1\le k\le n}$, equipped with the norm $\|\mathbf{U}\| = \sup_{\mathfrak{I}\in[0,T]} |\mathbf{U}(\mathfrak{I})|$. Additionally, let $\Phi = (\Upsilon^5, \|\mathbf{U}\|)$ represent a Banach space, where

$$\|\mathbf{U}\| = \sup_{\mathfrak{I}\in[0,T]} (|W| + |S| + |I_p| + |T|). \tag{3.5}$$

The results of the existence are established using Schauder's fixed point theorem in the following theorem.

Theorem 3.1. *Let $Z \in \Phi$ be a continuous function, and assume there exists a positive constant $V > 0$ such that.*

$$|Z(\mathfrak{I}, \mathbf{U}(\mathfrak{I}))| \le V(1 + |\mathbf{U}|), \quad \forall \mathfrak{I} \in [0,T],\ \mathbf{U} \in \Phi.$$

It follows that:

$$\nabla_1 = \left(\frac{(1-\varsigma)\Gamma(\varsigma)V + VT^{\varsigma}}{M(\varsigma)\Gamma(\varsigma)} \right) < 1. \tag{3.6}$$

Thus, the solution to Eq (3.4) is both unique and continuous for all $\mathfrak{I} \in [0,T]$.

Proof. From Eq (3.6), the solution to the stated problem is equivalent to the solution of the integral equation (3.4). Define the operator $\mho : \Phi \to \Phi$ as:

$$(\mho\mathbf{U})(\mathfrak{I}) = \mathbf{U}_0 + \frac{1-\varsigma}{M(\varsigma)} Z(\mathfrak{I}, \mathbf{U}(\mathfrak{I})) + \frac{\varsigma}{M(\varsigma)\Gamma(\varsigma)} \int_0^{\mathfrak{I}} (\mathfrak{I}-\varphi)^{\varsigma-1} Z(\lambda, \mathbf{U}(\lambda)) d\lambda. \tag{3.7}$$

Let $\mathbb{B}_{\varrho} = \{\mathbf{U} \in \lambda : \|\mathbf{U}\| \le \varrho,\ \ \varrho > 0\}$ denote a bounded, closed, and convex ball, where:

$$\varrho \ge \frac{\nabla_2}{1-\nabla_1}, \quad \text{and} \quad \nabla_2 = |\mathbf{U}_0| + \frac{1-\varsigma}{M(\varsigma)} V + \frac{T^{\varsigma}}{M(\varsigma)\Gamma(\varsigma)} V. \tag{3.8}$$

To complete the proof, it suffices to show that $(\mho(\mathbb{B}_{\varrho})) \subset \mathbb{B}_{\varrho}$, for all $t \in [0,T]$, as follows:

$$\begin{aligned} |(\mho\mathbf{U})(\mathfrak{I})| &\le |\mathbf{U}_0| + \frac{1-\varsigma}{M(\varsigma)} |Z(\mathfrak{I}, \mathbf{U}(\mathfrak{I}))| + \frac{\varsigma}{M(\varsigma)\Gamma(\varsigma)} \int_0^{\mathfrak{I}} (\mathfrak{I}-\lambda)^{\varsigma-1} |Z(\lambda, \mathbf{U}(\lambda))| d\lambda \\ &\le |\mathbf{U}_0| + \frac{1-\varsigma}{M(\varsigma)} V(1 + |\mathbf{U}(\mathfrak{I})|) + \frac{\varsigma}{M(\varsigma)\Gamma(\varsigma)} \int_0^{\mathfrak{I}} (\mathfrak{I}-\lambda)^{\varsigma-1} V(1 + |\mathbf{U}(\mathfrak{I})|) d\lambda, \end{aligned} \tag{3.9}$$

where $\mathbf{U} \in \mathbb{B}_{\varrho}$. Hence, the desired result is obtained:

$$\begin{aligned} \|(\mho\mathbf{U})\| &\le |\mathbf{U}_0| + \frac{1-\varsigma}{M(\varsigma)} V(1 + \|\mathbf{U}(\mathfrak{I})\|) + \frac{T^{\varsigma}}{M(\varsigma)\Gamma(\varsigma)} V(1 + \|\mathbf{U}(\mathfrak{I})\|) \\ &\le |\mathbf{U}_0| + \frac{1-\varsigma}{M(\varsigma)} V + \frac{T^{\varsigma}}{M(\varsigma)\Gamma(\varsigma)} V + \left[\frac{1-\varsigma}{M(\varsigma)} V + \frac{T^{\varsigma}}{M(\varsigma)\Gamma(\varsigma)} V \right] \varrho \end{aligned}$$

$$\leq \quad \nabla_2 + \nabla_1 \varrho \leq \varrho.$$

We have proven that $(\mho\mathbb{B}_\varrho) \subset \mathbb{B}_\varrho$.

Next, to show that the operator $\mho$ is continuous, let $\{\mathbf{U}_n\}$ be a sequence such that $\mathbf{U}_n \to \mathbf{U}$ in $\mathbb{B}_\varrho$ as $n \to \infty$. Then, for all $\mathfrak{I} \in [0, T]$, we have:

$$\begin{aligned}
\left|(\mho\mathbf{U}_n)(\mathfrak{I}) - (\mho\mathbf{U})(\mathfrak{I})\right| &\leq \frac{1-\varsigma}{M(\varsigma)}\left|Z(\mathfrak{I}, \mathbf{U}_n(\mathfrak{I})) - Z(\mathfrak{I}, \mathbf{U}(\mathfrak{I}))\right| + \\
&\quad \frac{\varsigma}{M(\varsigma)\Gamma(\varsigma)}\int_0^{\mathfrak{I}} (\mathfrak{I}-\lambda)^{\varsigma-1}\left|Z(\lambda, \mathbf{U}_n(\lambda)) - Z(\lambda, \mathbf{U}(\lambda))\right| d\lambda \\
&\leq \frac{1-\varsigma}{M(\varsigma)}\|Z(\mathfrak{I}, \mathbf{U}_n(\mathfrak{I})) - Z(\mathfrak{I}, \mathbf{U}(\mathfrak{I}))\| + \\
&\quad \frac{T^\varsigma}{M(\varsigma)\Gamma(\varsigma)}\|Z(\lambda, \mathbf{U}_n(\lambda)) - Z(\lambda, \mathbf{U}(\lambda))\|.
\end{aligned}$$

From the continuity of the function Z, it follows that:

$$\|(\mho\mathbf{U}_n)(\mathfrak{I}) - (\mho\mathbf{U})(\mathfrak{I})\| \to 0 \quad \text{as} \quad n \to \infty. \tag{3.10}$$

Thus, $\mho$ is continuous on $\mathbb{B}_\varrho$.

To conclude, we establish that $(\mho\mathbb{B}_\varrho)$ is a relatively compact operator. As $(\mho\mathbb{B}_\varrho) \subset \mathbb{B}_\varrho$, it follows that the operator is uniformly bounded. Furthermore, we demonstrate that $\mho$ is "equi-continuous" on $\mathbb{B}_\varrho$. Let $\mathbf{U} \in \mathbb{B}_\varrho$, and take $\mathfrak{I}_1, \mathfrak{I}_2 \in [0, T]$ such that $\mathfrak{I}_1 < \mathfrak{I}_2$. Then, the following holds:

$$\begin{aligned}
\|\mho\mathbf{U}(\mathfrak{I}_2) - \mho\mathbf{U}(\mathfrak{I}_1)\| &\leq \frac{1-\varsigma}{M(\varsigma)}\left|Z(\mathfrak{I}_2, \mathbf{U}(\mathfrak{I}_2)) - Z(\mathfrak{I}_1, \mathbf{U}(\mathfrak{I}_1))\right| \\
&+ \frac{\varsigma}{M(\varsigma)\Gamma(\varsigma)}\left|\left[\int_0^{\mathfrak{I}_2} (\mathfrak{I}_2-\lambda)^{\varsigma-1} - \int_0^{\mathfrak{I}_1} (\mathfrak{I}_1-\lambda)^{\varsigma-1}\right] Z(\lambda, \mathbf{U}(\lambda)) d\lambda\right| \\
&\leq \frac{1-\varsigma}{M(\varsigma)}\left|Z(\mathfrak{I}_2, \mathbf{U}(\mathfrak{I}_2)) - Z(\mathfrak{I}_1, \mathbf{U}(\mathfrak{I}_1))\right| + \frac{\varsigma}{M(\varsigma)}\frac{L(1+\|\mathbf{U}\|)}{\Gamma(\varsigma+1)}(\mathfrak{I}_2^\varsigma - \mathfrak{I}_1^\varsigma).
\end{aligned}$$

It is evident that $\|\mho\mathbf{U}(\mathfrak{I}_2) - \mho\mathbf{U}(\mathfrak{I}_1)\| \to 0$ as $\mathfrak{I}_2 \to \mathfrak{I}_1$. Using the Arzelà–Ascoli theorem, it follows that $(\mho\mathbb{B}_\varrho)$ is relatively compact, which ensures that the operator $\mho$ is completely continuous. As a result, the problem (1.1) has at least one solution.

We now turn to the uniqueness of the solution for the proposed model (1.1), which is established under the following conditions:

$$0 \leq \left[1 - \frac{1-\varsigma}{M(\varsigma)}\varrho - \frac{\varsigma T^\varsigma}{M(\varsigma)\Gamma(\varsigma)}\varrho\right]. \tag{3.11}$$

If additional potential solutions, such as W, S, I_p, N, are assumed to exist, it can be concluded that:

$$W(\mathfrak{I}) - W_1(\mathfrak{I}) = \frac{1-\varsigma}{M(\varsigma)}(\mathbf{F}_1(\mathfrak{I}, W) - \mathbf{F}_1(\mathfrak{I}, W)) + \frac{\varsigma}{M(\varsigma)\Gamma(\varsigma)}\int_0^{\mathfrak{I}} (\mathbf{F}_1(\lambda, W) - \mathbf{F}_1(\lambda, L_1))d\lambda, \tag{3.12}$$

and using norm to Eq (3.12), we have

$$\begin{aligned}\|W - W_1\| &= \left\|\frac{1-\varsigma}{M(\varsigma)}(\mathbf{F}_1(t,W) - \mathbf{F}_1(\mathfrak{I},W_1)) + \frac{\varsigma}{M(\varsigma)\Gamma(\varsigma)}\int_0^{\mathfrak{I}}(\mathbf{F}_1(\lambda,W) - \mathbf{F}_1(\lambda,W_1))d\lambda\right\| \\ &\leq \frac{1-\varsigma}{M(\varsigma)}\varrho\|W - W_1\| + \frac{\varsigma}{M(\varsigma)\Gamma(\varsigma)}\varrho\|W - W_1\|. \end{aligned} \tag{3.13}$$

Therefore,

$$\|W - W_1\|\left[1 - \frac{1-\varsigma}{M(\varsigma)}\varrho - \frac{\varsigma T^{\varsigma}}{M(\varsigma)\Gamma(\varsigma)}\varrho\right] \leq 0. \tag{3.14}$$

This implies that $W = W_1$, provided the inequality (3.11) holds. Similarly, for the other compartments, if $S = S_1$, $I_p = I_{P_1}$, and $N = N_1$, the solution is guaranteed to be unique. □

We now establish the UH stability for the proposed system (1.1).

Theorem 3.2. *Let $Z \in \lambda$ be a continuous function, and suppose there exists a constant $\mathcal{K} > 0$ such that*

$$\left|Z(\mathfrak{I},\mathcal{Q}) - Z(\mathfrak{I},\widetilde{\mathcal{Q}})\right| \leq \mathcal{K}\left|\mathcal{Q} - \widetilde{\mathcal{Q}}\right|, \quad \forall \mathfrak{I} \in [0,T],\ \mathcal{Q} \in \lambda,$$

where the following condition holds:

$$1 > \frac{(1-\varsigma)\Gamma(\varsigma)\mathcal{K} + \mathcal{K}T^{\varsigma}}{M(\varsigma)\Gamma(\varsigma)}.$$

Let $\mathcal{Q}$ and $\widetilde{\mathcal{Q}}$ represent the solutions of Eq (3.2). Then, we have:

$${}^{\mathcal{ABC}}\mathbf{D}_{\mathfrak{I}}^{\varsigma}\widetilde{\mathcal{Q}}(\mathfrak{I}) = Z(\mathfrak{I},\widetilde{\mathcal{Q}}(\mathfrak{I})), \quad \widetilde{\mathcal{Q}}(0) = \mathcal{Q}_0 + \varepsilon \geq 0. \tag{3.15}$$

where

$$\begin{cases} \tilde{\mathcal{Q}} = (\tilde{W},\tilde{S},\tilde{I}_p,\tilde{N})^T, \\ \mathcal{Q}_0 + \varepsilon = (W_0 + \varepsilon, S_0 + \varepsilon, I_{P_0} + \varepsilon, N_0 + \varepsilon, \\ Z(\mathfrak{I},\tilde{\mathcal{Q}}(t)) = \mathbf{F}_i(\tilde{W},\tilde{S},\tilde{I}_p,\tilde{N})^T, \ \ i = 1,2,3,4. \end{cases} \tag{3.16}$$

Then,

$$\|\mathcal{Q} - \tilde{\mathcal{Q}}\| \leq \left[1 - \frac{(1-\varsigma)\Gamma(\varsigma)\mathcal{K} + \mathcal{K}T^{\varsigma}}{M(\varsigma)\Gamma(\varsigma)}\right]^{-1}|\varepsilon|. \tag{3.17}$$

Proof. The solutions to the given problem (3.2) and Eq (3.15) correspond to the integral Eq (3.4):

$$\tilde{\mathcal{Q}}(\mathfrak{I}) = \mathcal{Q}_0 + \varepsilon + \frac{1-\varsigma}{M(\varsigma)}Z(\mathfrak{I},\tilde{\mathcal{Q}}(\mathfrak{I})) + \frac{\varsigma}{M(\varsigma)\Gamma(\varsigma)}\int_0^{\mathfrak{I}}(\mathfrak{I} - \lambda)^{\varsigma-1}Z(\lambda,\tilde{\mathcal{Q}}(\lambda))\,d\lambda, \tag{3.18}$$

for all $\mathfrak{I} \in [0,T]$. From this, we obtain:

$$\begin{aligned}|\mathcal{Q} - \tilde{\mathcal{Q}}| &\leq |\varepsilon| + \frac{1-\varsigma}{M(\varsigma)}\left|Z(\mathfrak{I},\mathcal{Q}(\mathfrak{I})) - Z(\mathfrak{I},\tilde{\mathcal{Q}}(\mathfrak{I}))\right| \\ &+ \frac{\varsigma}{M(\varsigma)\Gamma(\varsigma)}\int_0^{\mathfrak{I}}(\mathfrak{I} - \lambda)^{\varsigma-1}\left|Z(\lambda,\mathcal{Q}(\lambda)) - Z(\lambda,\tilde{\mathcal{Q}}(\lambda))\right|d\lambda \end{aligned}$$

$$\begin{aligned} &\leq |\varepsilon| + \frac{1-\varsigma}{M(\varsigma)}\mathcal{K}\left|\mathcal{Q}(\mathfrak{I}) - \tilde{\mathcal{Q}}(\mathfrak{I})\right| + \frac{\varsigma}{M(\varsigma)\Gamma(\varsigma)}\int_0^{\mathfrak{I}}(\mathfrak{I}-\lambda)^{\varsigma-1}\mathcal{K}\left|\mathcal{Q}(\lambda) - \tilde{\mathcal{Q}}(\lambda)\right| d\lambda \\ &\leq |\varepsilon| + \left[\frac{1-\varsigma}{M(\varsigma)} + \frac{T^{\varsigma}}{M(\varsigma)\Gamma(\varsigma)}\right]\mathcal{K}\|\mathcal{Q} - \tilde{\mathcal{Q}}\|. \end{aligned}$$

Hence, we deduce:

$$\|\mathcal{Q} - \tilde{\mathcal{Q}}\| \leq |\varepsilon| + \left[\frac{(1-\varsigma)\Gamma(\varsigma) + T^{\varsigma}}{M(\varsigma)\Gamma(\varsigma)}\right]\mathcal{K}\|\mathcal{Q} - \tilde{\mathcal{Q}}\|.$$

Thus:

$$\|\mathcal{Q} - \tilde{\mathcal{Q}}\| \leq \left[1 - \frac{(1-\varsigma)\Gamma(\varsigma)\mathcal{K} + \mathcal{K}T^{\varsigma}}{M(\varsigma)\Gamma(\varsigma)}\right]^{-1}|\varepsilon|.$$

This completes the proof of the theorem.

□

4. Numerical approach

This section highlights a computational method designed to solve the stated problem, where the time derivative is modeled as a fractional derivative with the generalized ML kernel. The simulation employs an interpolation polynomial to estimate the fractional-order integral. To achieve this, the renowned AB approach is applied [28].

By incorporating the initial conditions and using the operator ${}^{ABC}\mathbf{I}_0^{\varsigma}$, the numerical scheme for the given problem is constructed as follows:

$$\begin{cases} W - W_0 &= {}^{ABC}\mathbf{I}_0^{\varsigma}\mathbf{G}_1(W, \mathfrak{I}), \\ S - S_0 &= {}^{ABC}\mathbf{I}_0^{\varsigma}\mathbf{G}_2(S, \mathfrak{I}), \\ I_p - I_{p0} &= {}^{ABC}\mathbf{I}_0^{\varsigma}\mathbf{G}_3(I_p, \mathfrak{I}), \\ N - N_0 &= {}^{ABC}\mathbf{I}_0^{\varsigma}\mathbf{G}_4(N, \mathfrak{I}), \end{cases} \tag{4.1}$$

which gives

$$\begin{aligned} W(\mathfrak{I}) - W_0 &= \frac{1-\varsigma}{M(\varsigma)}\mathbf{G}_1(W(\mathfrak{I}), \mathfrak{I}) + \frac{\varsigma}{M(\varsigma)\Gamma(\varsigma)}\int_0^{\mathfrak{I}}(\mathfrak{I}-\lambda)^{\varsigma-1}\mathbf{G}_1(W(\lambda), \lambda)d\lambda, \\ S(\mathfrak{I}) - S_0 &= \frac{1-\varsigma}{M(\varsigma)}\mathbf{G}_2(S(\mathfrak{I}), \mathfrak{I}) + \frac{\varsigma}{M(\varsigma)\Gamma(\varsigma)}\int_0^{\mathfrak{I}}(\mathfrak{I}-\lambda)^{\varsigma-1}\mathbf{G}_2(S(\lambda), \lambda)d\lambda, \\ I_p(\mathfrak{I}) - I_{p0} &= \frac{1-\varsigma}{M(\varsigma)}\mathbf{G}_3(I_p(\mathfrak{I}), \mathfrak{I}) + \frac{\varsigma}{M(\varsigma)\Gamma(\varsigma)}\int_0^{\mathfrak{I}}(\mathfrak{I}-\lambda)^{\varsigma-1}\mathbf{G}_3(I_p(\lambda), \lambda)d\lambda, \\ N(\mathfrak{I}) - N_0 &= \frac{1-\varsigma}{M(\varsigma)}\mathbf{G}_4(N(\mathfrak{I}), \mathfrak{I}) + \frac{\varsigma}{M(\varsigma)\Gamma(\varsigma)}\int_0^{\mathfrak{I}}(\mathfrak{I}-\lambda)^{\varsigma-1}\mathbf{G}_4(N(\lambda), \lambda)d\lambda. \end{aligned}$$

An iterative scheme is developed by substituting $\mathfrak{I} = \mathfrak{I}_{\iota+1}$ for $\nu = 0, 1, 2, \ldots$ into the specified

system:

$$\begin{cases} W(\mathfrak{I}_{\nu+1}) - W(0) &= \frac{1-\varsigma}{M(\varsigma)}\mathbf{G}_1(W(\mathfrak{I}_\nu), t_\nu) + \frac{\varsigma}{M(\varsigma)\Gamma(\varsigma)}\sum_{i=0}^{\nu}\int_{\mathfrak{I}_i}^{\mathfrak{I}_{i+1}}(\mathfrak{I}_{\nu+1}-\lambda)^{\varsigma-1}\mathbf{G}_1(L(\lambda),\lambda)d\lambda, \\ S(\mathfrak{I}_{\nu+1}) - S(0) &= \frac{1-\varsigma}{M(\varsigma)}\mathbf{G}_2(S(\mathfrak{I}_\nu), \mathfrak{I}_\nu) + \frac{\varsigma}{M(\varsigma)\Gamma(\varsigma)}\sum_{i=0}^{\nu}\int_{\mathfrak{I}_i}^{\mathfrak{I}_{i+1}}(\mathfrak{I}_{\nu+1}-\lambda)^{\varsigma-1}\mathbf{G}_2(S(\lambda),\lambda)d\lambda, \\ I_p(\mathfrak{I}_{\nu+1}) - I_p(0) &= \frac{1-\varsigma}{M(\varsigma)}\mathbf{G}_3(I_p(\mathfrak{I}_\nu), \mathfrak{I}_\nu) + \frac{\varsigma}{M(\varsigma)\Gamma(\varsigma)}\sum_{i=0}^{\nu}\int_{\mathfrak{I}_i}^{\mathfrak{I}_{i+1}}(\mathfrak{I}_{\nu+1}-\lambda)^{\varsigma-1}\mathbf{G}_3(I_p(\lambda),\lambda)d\lambda, \\ N(\mathfrak{I}_{\nu+1}) - N(0) &= \frac{1-\varsigma}{M(\varsigma)}\mathbf{G}_4(N(\mathfrak{I}_\nu), \mathfrak{I}_\nu) + \frac{\varsigma}{M(\varsigma)\Gamma(\varsigma)}\sum_{i=0}^{\nu}\int_{\mathfrak{I}_i}^{\mathfrak{I}_{i+1}}(\mathfrak{I}_{\nu+1}-\lambda)^{\varsigma-1}\mathbf{G}_4(N(\lambda),\lambda)d\lambda. \end{cases}$$

To approximate the functions $\mathbf{G}_1(W(\lambda),\lambda)$, $\mathbf{G}_2(S(\lambda),\lambda)$, $\mathbf{G}_3(I_p(\lambda),\lambda)$, and $\mathbf{G}_4(N(\lambda),\lambda)$, a two-step interpolation polynomial is employed. The integral in the above equation is evaluated over the interval $[\mathfrak{I}_\varkappa, \mathfrak{I}_{\varkappa+1}]$. We then obtain:

$$\begin{cases} \mathbf{G}_1(W(\lambda),\lambda) &\cong \frac{\mathbf{G}_1(W(\mathfrak{I}_\varkappa),\mathfrak{I}_\varkappa)}{\Delta}(\mathfrak{I}-\mathfrak{I}_{\varkappa-1}) + \frac{\mathbf{G}_1(W(\mathfrak{I}_{\varkappa-1}),\mathfrak{I}_{\varkappa-1})}{\Delta}(\mathfrak{I}-\mathfrak{I}_\varkappa), \\ \mathbf{G}_2(S(\lambda),\lambda) &\cong \frac{\mathbf{G}_2(S(\mathfrak{I}_\varkappa),\mathfrak{I}_\varkappa)}{\Delta}(\mathfrak{I}-\mathfrak{I}_{\varkappa-1}) + \frac{\mathbf{G}_2(S(\mathfrak{I}_{\varkappa-1}),\mathfrak{I}_{\varkappa-1})}{\Delta}(\mathfrak{I}-\mathfrak{I}_\varkappa), \\ \mathbf{G}_3(I_p(\lambda),\lambda) &\cong \frac{\mathbf{G}_3(I_p(\mathfrak{I}_\varkappa),\mathfrak{I}_\varkappa)}{\Delta}(\mathfrak{I}-\mathfrak{I}_{\varkappa-1}) + \frac{\mathbf{G}_3(I_p(\mathfrak{I}_{\varkappa-1}),\mathfrak{I}_{\varkappa-1})}{\Delta}(\mathfrak{I}-\mathfrak{I}_\varkappa), \\ \mathbf{G}_4(N(\lambda),\lambda) &\cong \frac{\mathbf{G}_4(N(\mathfrak{I}_\varkappa),\mathfrak{I}_\varkappa)}{\Delta}(\mathfrak{I}-\mathfrak{I}_{\varkappa-1}) + \frac{\mathbf{G}_4(N(\mathfrak{I}_{\varkappa-1}),\mathfrak{I}_{\varkappa-1})}{\Delta}(\mathfrak{I}-\mathfrak{I}_\varkappa), \end{cases} \tag{4.2}$$

which gives

$$\begin{aligned} W(\mathfrak{I}_{\iota+1}) &= W(0) + \frac{1-\varsigma}{M(\varsigma)}\mathbf{G}_1(W(\mathfrak{I}_\nu),\mathfrak{I}_\nu) + \frac{\varsigma}{M(\varsigma)\Gamma(\varsigma)}\sum_{i=0}^{\nu}\left(\frac{\mathbf{G}_1(W(\mathfrak{I}_\varkappa),\mathfrak{I}_\varkappa)}{\Delta}I_{\varkappa-1,\varsigma} + \frac{\mathbf{G}_1(L(\mathfrak{I}_{\varkappa-1}),\mathfrak{I}_{\varkappa-1})}{\Delta}I_{\varkappa,\varsigma}\right), \\ S(\mathfrak{I}_{\iota+1}) &= S(0) + \frac{1-\varsigma}{M(\varsigma)}\mathbf{G}_2(S(\mathfrak{I}_\nu),\mathfrak{I}_\nu) + \frac{\varsigma}{M(\varsigma)\Gamma(\varsigma)}\sum_{i=0}^{\nu}\left(\frac{\mathbf{G}_2(S(\mathfrak{I}_\varkappa),\mathfrak{I}_\varkappa)}{\Delta}I_{\varkappa-1,\varsigma} + \frac{\mathbf{G}_2(S(\mathfrak{I}_{\varkappa-1}),\mathfrak{I}_{\varkappa-1})}{\Delta}I_{\varkappa,\varsigma}\right), \\ I_p(\mathfrak{I}_{\iota+1}) &= I_p(0) + \frac{1-\varsigma}{M(\varsigma)}\mathbf{G}_3(I_p(\mathfrak{I}_\nu),\mathfrak{I}_\nu) + \frac{\varsigma}{M(\varsigma)\Gamma(\varsigma)}\sum_{i=0}^{\nu}\left(\frac{\mathbf{G}_3(I_p(\mathfrak{I}_\varkappa),\mathfrak{I}_\varkappa)}{\Delta}I_{\varkappa-1,\varsigma} + \frac{\mathbf{G}_3(I_p(\mathfrak{I}_{\varkappa-1}),\mathfrak{I}_{\varkappa-1})}{\Delta}I_{\varkappa,\varsigma}\right), \\ T(\mathfrak{I}_{\iota+1}) &= N(0) + \frac{1-\varsigma}{M(\varsigma)}\mathbf{G}_4(N(\mathfrak{I}_\nu),\mathfrak{I}_\nu) + \frac{\varsigma}{M(\varsigma)\Gamma(\varsigma)}\sum_{i=0}^{\nu}\left(\frac{\mathbf{G}_4(N(\mathfrak{I}_\varkappa),\mathfrak{I}_\varkappa)}{\Delta}I_{\varkappa-1,\varsigma} + \frac{\mathbf{G}_4(N(\mathfrak{I}_{\varkappa-1}),\mathfrak{I}_{\varkappa-1})}{\Delta}I_{\varkappa,\varsigma}\right), \end{aligned} \tag{4.3}$$

where

$$I_{\varkappa-1,\varsigma} = \int_{\mathfrak{I}_\varkappa}^{\mathfrak{I}_{\varkappa+1}}(\mathfrak{I}-\mathfrak{I}_{\varkappa-1})(\mathfrak{I}_{\iota+1}-\mathfrak{I})^{\varsigma-1}d\mathfrak{I}, \quad I_{\varkappa,\varsigma} = \int_{\mathfrak{I}_\varkappa}^{\mathfrak{I}_{\varkappa+1}}(\mathfrak{I}-\mathfrak{I}_\iota)(\mathfrak{I}_{\iota+1}-\mathfrak{I})^{\varsigma-1}d\mathfrak{I}.$$

The integrals $I_{\varkappa-1,\varsigma}$ and $I_{\varkappa,\varsigma}$ are computed as shown below:

$$\begin{aligned} I_{\varkappa-1,\varsigma} &= -\frac{1}{\varsigma}\Big[(\mathfrak{I}_{\varkappa+1}-\mathfrak{I}_{\varkappa-1})(\mathfrak{I}_{\iota+1}-\mathfrak{I}_{\varkappa+1})^{\varsigma} - (\mathfrak{I}_\varkappa-\mathfrak{I}_{\varkappa-1})(\mathfrak{I}_{\iota+1}-\mathfrak{I}_\varkappa)^{\varsigma}\Big] \\ &\quad -\frac{1}{\varsigma(\varsigma-1)}\Big[(\mathfrak{I}_{\iota+1}-\mathfrak{I}_{\varkappa+1})^{\varsigma+1} - (\mathfrak{I}_{\iota+1}-\mathfrak{I}_\varsigma)^{\varsigma+1}\Big], \end{aligned}$$

and

$$I_{\varkappa,\varsigma} = -\frac{1}{\varsigma}\Big[(\mathfrak{I}_{\varkappa+1}-\mathfrak{I}_i)(\mathfrak{I}_{\iota+1}-\mathfrak{I}_{\varkappa+1})^{\varsigma}\Big] - \frac{1}{\varkappa(\varkappa-1)}\Big[(\mathfrak{I}_{\iota+1}-\mathfrak{I}_{\varkappa+1})^{\varsigma+1} - (\mathfrak{I}_{\iota+1}-\mathfrak{I}_\varkappa)^{\varsigma+1}\Big],$$

where $\Im_\varsigma = i\Delta$. From this, we find:

$$I_{\varkappa-1,\varsigma} = -\frac{\Delta^{\varsigma+1}}{\varsigma(\varsigma+1)}\Big[(\iota+1-\varkappa)^{\varsigma}(\iota-\varkappa+2+\varsigma)-(\iota-\varkappa)^{\varsigma}(\iota-\varkappa+2+2\varsigma)\Big], \tag{4.4}$$

and

$$I_{\varkappa,\varsigma} = \frac{\Delta^{\varsigma+1}}{\varsigma(\varsigma+1)}\Big[(\iota+1-\varkappa)^{\varsigma+1}-(\iota-\varkappa)^{\varsigma}(\iota-\varkappa+1+\varsigma)\Big]. \tag{4.5}$$

By inserting Eqs (4.4) and (4.5) into Eq (4.3), the following is derived:

$$\begin{aligned} W(\Im_{\iota+1}) &= L(\Im_0)+\frac{(1-\varsigma)}{M(\varsigma)}\Big[\mathbf{G}_1(W(\Im_\iota),\Im_\iota)\Big]+\frac{\varsigma}{M(\varsigma)}\sum_{i=0}^{\nu}\Big(\frac{\mathbf{G}_1(W(\Im_\iota),\Im_\iota)}{\Gamma(\varsigma+2)}\\ &\quad\times\Delta^{\varsigma}\Big[(\iota+1-\varkappa)^{\varsigma}(\iota-\varkappa+2+\varsigma)-(\iota-\varkappa)^{\varsigma}(\iota-\varkappa+2+2\varsigma)\Big]\\ &\quad-\frac{\mathbf{G}_1(W(\Im_{\nu-1}),\Im_{\nu-1})}{\Gamma(\varsigma+2)}\Delta^{\varsigma}[(\iota+1-\varkappa)^{\varsigma+1}-(\iota-\varkappa)^{\varsigma}(\iota-\varkappa+1+\varsigma)]\Big), \end{aligned} \tag{4.6}$$

$$\begin{aligned} S(\Im_{\iota+1}) &= S(\Im_0)+\frac{(1-\varsigma)}{M(\varsigma)}\Big[\mathbf{G}_2(S(\Im_\iota),\Im_\iota)\Big]+\frac{\varsigma}{M(\varsigma)}\sum_{i=0}^{\nu}\Big(\frac{\mathbf{G}_2(S(\Im_\iota),\Im_\iota)}{\Gamma(\varsigma+2)}\\ &\quad\times\Delta^{\varsigma}\Big[(\iota+1-\varkappa)^{\varsigma}(\iota-\varkappa+2+\varsigma)-(\iota-\varkappa)^{\varsigma}(\iota-\varkappa+2+2\varsigma)\Big]\\ &\quad-\frac{\mathbf{G}_2(S(\Im_{\nu-1}),\Im_{\nu-1})}{\Gamma(\varsigma+2)}\Delta^{\varsigma}[(\iota+1-\varkappa)^{\varsigma+1}-(\iota-\varkappa)^{\varsigma}(\iota-\varkappa+1+\varsigma)]\Big), \end{aligned} \tag{4.7}$$

$$\begin{aligned} I_p(\Im_{\iota+1}) &= I_p(\Im_0)+\frac{(1-\varsigma)}{M(\varsigma)}\Big[\mathbf{G}_3(I_p(\Im_\iota),\Im_\iota)\Big]+\frac{\varsigma}{M(\varsigma)}\sum_{i=0}^{\nu}\Big(\frac{\mathbf{G}_3(I_p(\Im_\iota),\Im_\iota)}{\Gamma(\varsigma+2)}\\ &\quad\times\Delta^{\varsigma}\Big[(\iota+1-\varkappa)^{\varsigma}(\iota-\varkappa+2+\varsigma)-(\iota-\varkappa)^{\varsigma}(\iota-\varkappa+2+2\varsigma)\Big]\\ &\quad-\frac{\mathbf{G}_3(I_p(\Im_{\nu-1}),\Im_{\nu-1})}{\Gamma(\varsigma+2)}\Delta^{\varsigma}[(\iota+1-\varkappa)^{\varsigma+1}-(\iota-\varkappa)^{\varsigma}(\iota-\varkappa+1+\varsigma)]\Big), \end{aligned} \tag{4.8}$$

$$\begin{aligned} N(\Im_{\iota+1}) &= T(\Im_0)+\frac{(1-\varsigma)}{M(\varsigma)}\Big[\mathbf{G}_4(N(\Im_\iota),\Im_\iota)\Big]+\frac{\varsigma}{M(\varsigma)}\sum_{i=0}^{\nu}\Big(\frac{\mathbf{G}_4(N(\Im_\iota),\Im_\iota)}{\Gamma(\varsigma+2)}\\ &\quad\times\Delta^{\varsigma}\Big[(\iota+1-\varkappa)^{\varsigma}(\iota-\varkappa+2+\varsigma)-(\iota-\varkappa)^{\varsigma}(\iota-\varkappa+2+2\varsigma)\Big]\\ &\quad-\frac{\mathbf{G}_4(N(\Im_{\nu-1}),\Im_{\nu-1})}{\Gamma(\varsigma+2)}\Delta^{\varsigma}[(\iota+1-\varkappa)^{\varsigma+1}-(\iota-\varkappa)^{\varsigma}(\iota-\varkappa+1+\varsigma)]\Big). \end{aligned} \tag{4.9}$$

4.1. Analysis and discussion of model simulation outcomes

This section presents graphical numerical simulations to validate the outcomes at various fractional-order levels. The results are compared with the data provided in Table 2 and the model's

initial conditions 1.1. Figure 1a illustrates the temporal dynamics of polluted water sources under different fractional orders. The simulations reveal an initial increase in pollution levels, followed by stabilization, where higher fractional orders better capture the long-term memory effects of contamination. Figure 1b represents the water sources susceptible to pollution, showing how exposure to contaminants increases over time before reaching a steady state. Figure 1c depicts the number of water sources actively contaminated by pollutants, demonstrating a rise in contamination before equilibrium is reached due to pollutant transport and accumulation. Finally, Figure 1d highlights the restoration of water sources through treatment interventions, with fractional models capturing a more gradual recovery process than integer-order models. These findings emphasize the significance of fractional calculus in accurately modeling water pollution dynamics and evaluating the effectiveness of remediation strategies.

Table 2. Parameters and their numerical values in model 1.1.

Notation	Value	Source	Notation	Value	Source
W	5	S	4	I_p	1
N	0	Λ	0.8	ρ	0.25
α_1	0.18	α_2	0.02	δ	0.30
μ	0.40	θ_1	0.20	θ_2	0.50

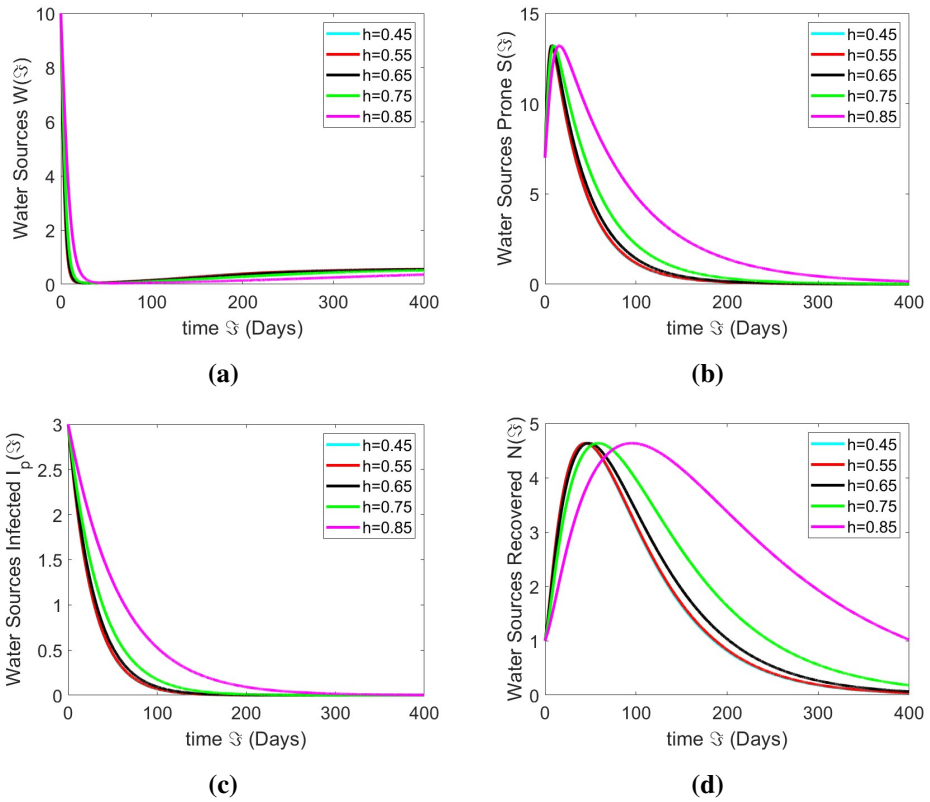

Figure 1. The numerical simulation graphs represent all compartments of the considered model.

The parameters used in the simulations were calibrated based on empirical values reported in previous studies on water contamination dynamics [27]. The transport rates (α_1, α_2) represent the movement of soluble and insoluble pollutants and were selected based on observed pollutant dispersion patterns. The treatment capacities (θ_1, θ_2) were assumed to ensure the model practical pollutant removal processes. The pollutant removal rate μ and conversion rate ρ were assumed according to environmental studies on degradation rates and contamination persistence. While this study primarily focuses on theoretical validation, future work will incorporate real-time water quality datasets for further empirical verification. We simulate the outcomes of the foregoing algorithms for the different categories using Matlab and the parameter values from Table 2 as shown in Figures 1–4.

The impact of varying fractional orders on pollution dynamics is primarily attributed to the memory effects inherent in fractional operators. Higher fractional orders enhance memory retention, causing pollution to persist longer and stabilizing more gradually. Unlike classical integer-order derivatives, the ABC fractional derivative models long-range interactions and historical dependence. In contrast, lower fractional orders reduce the memory effect, making the system behave more similarly to an integer-order model, leading to faster stabilization of pollution levels. These observations highlight the importance of fractional calculus in capturing realistic pollutant dispersion behaviors.

4.2. ANN implementation

ANNs play a pivotal role in advancing the analysis of water pollution dynamics, particularly when integrated with fractional differential models. This study uses ANNs to process data derived from the ABC fractional framework, enabling robust predictive analysis of pollution trends. The dataset is partitioned into 70% for training, 15% for testing, and 15% for validation, with each subset corresponding to different fractional-order scenarios. The ANN architecture consists of a multilayer perceptron (MLP) model featuring an input layer representing fractional-order pollution parameters, a hidden layer with 10 neurons, and an output layer predicting future water quality states. The network is trained using the Levenberg-Marquardt backpropagation algorithm, minimizing the mean squared error (MSE) to optimize predictive accuracy. Through an iterative learning process spanning 1000 epochs, the ANN achieves an exceptionally low MSE of 1.6669×10^{-11}, demonstrating strong alignment with simulation data, as indicated by a regression R-value close to 1. The ANN effectively models complex contamination dynamics and mitigation outcomes by capturing intricate patterns in pollutant transport rates, treatment capacities, and environmental variables. Moreover, its adaptability to varying fractional orders underscores its scalability and effectiveness as a data-driven water quality management and decision-making tool. The ANN framework is employed separately from the numerical AB method, focusing solely on analyzing the simulation outputs and forecasting pollution behavior. The AB method is utilized to approximate the fractional-order differential equations governing pollution dynamics numerically. At the same time, the ANN framework is independently applied to analyze simulation outputs and improve predictive accuracy, as illustrated in Figure 2a.

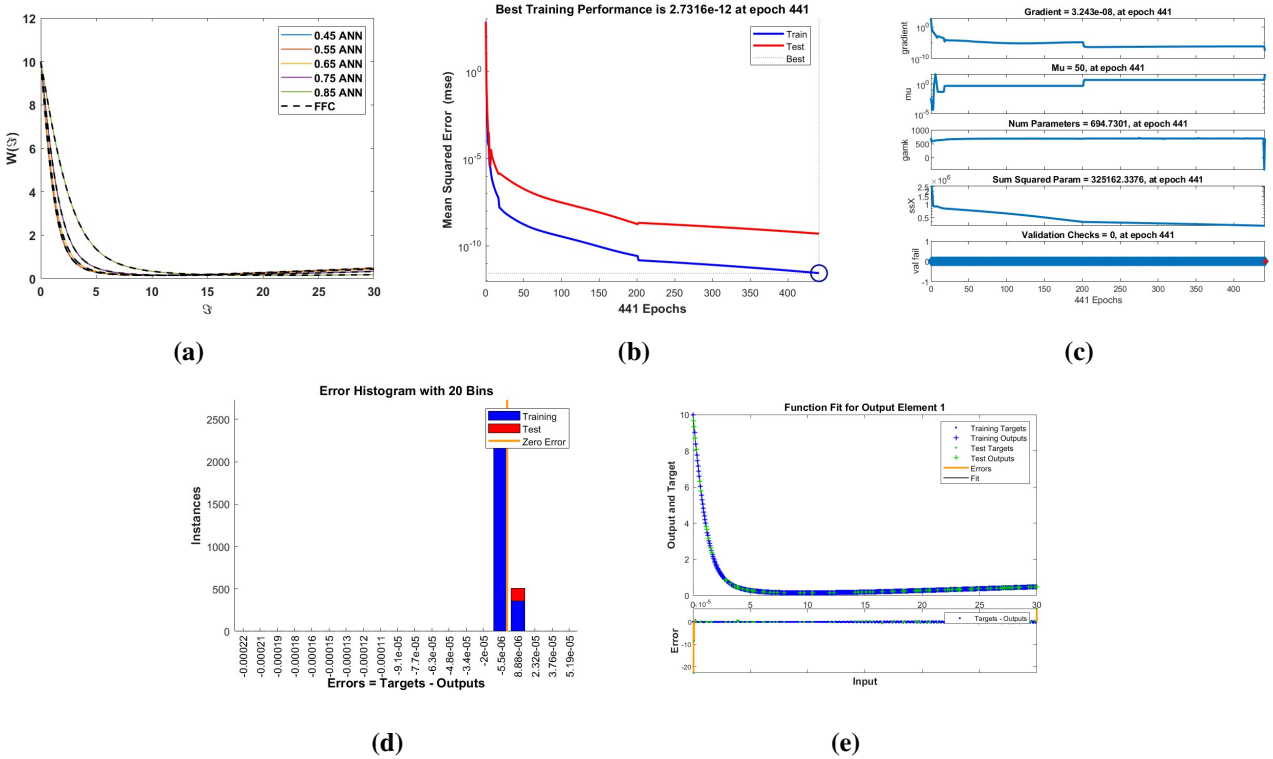

Figure 2. The statistical dynamics of the analyzed model comprise (a) a comparison, (b) the mean squared error, (c) regression analysis, (d) an error histogram, and (e) the ANN's training performance fit.

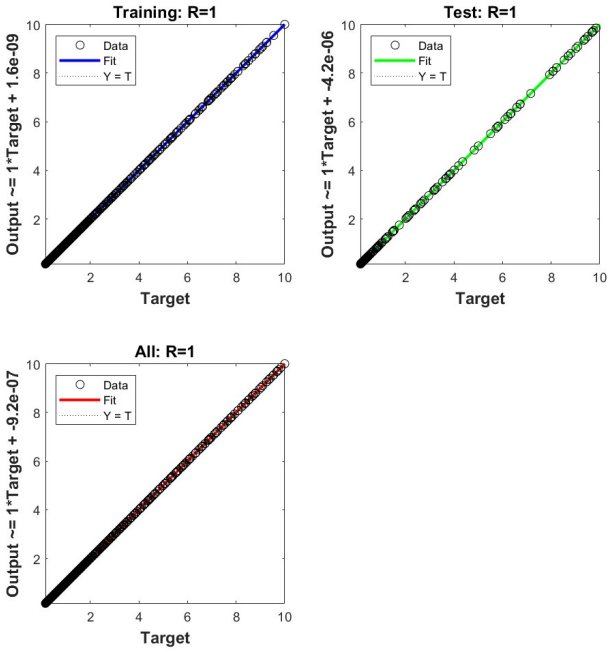

Figure 3. ANN-based regression was dynamically implemented to model the system's behavior being analyzed.

As demonstrated in Figure 4a, the ANN approach is applied separately from the AB method, which is used for numerically approximating the fractional-order differential equations. At epoch 877, the analyzed model achieves a mean squared error of $1.6414e-12$, as illustrated in Figure 4b. The training progression is displayed in Figure 6c. The error histogram, highlighting the best result of $1.58e-07$, is provided in Figure 4e. Additionally, Figure 4e showcases the optimal fit for testing and training datasets, along with the corresponding errors. The regression analysis for the model, covering all datasets—training, testing, and combined—is depicted in Figure 5. The results confirm that the model is effectively trained, with data points aligning closely along the regression line, resulting in an R value approximately equal to 1.

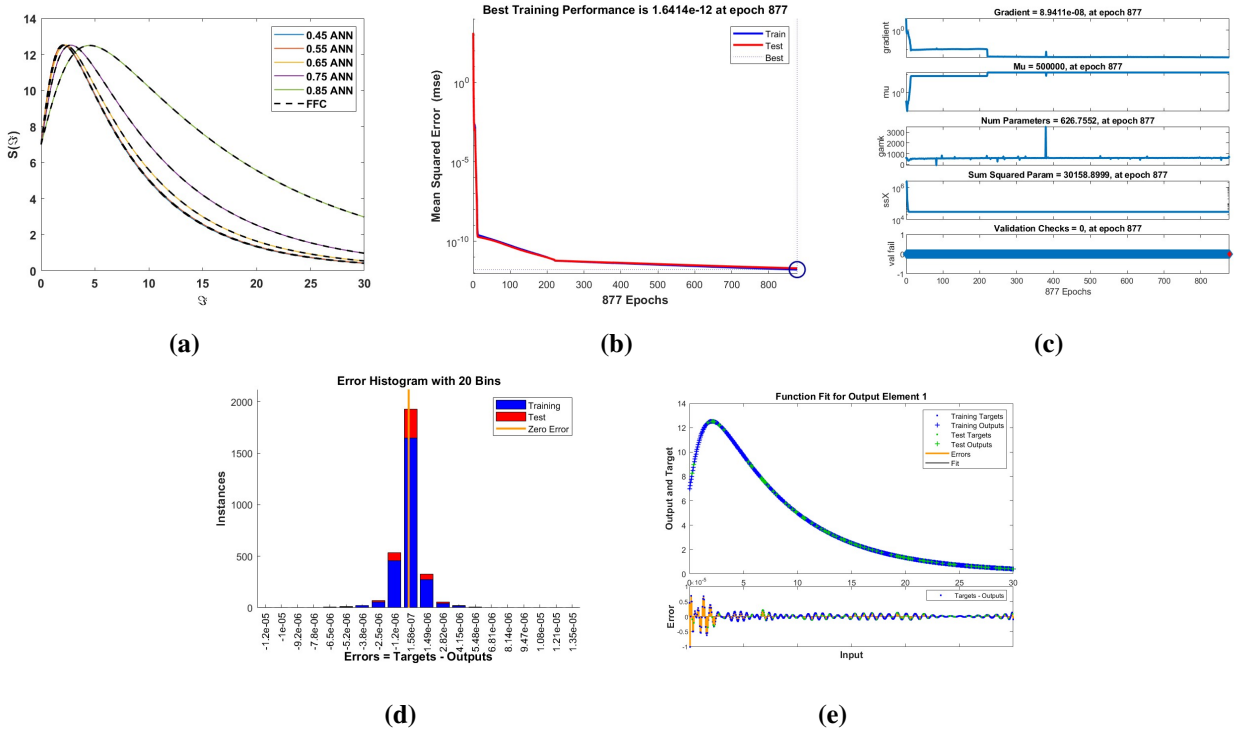

Figure 4. The statistical dynamics of the analyzed model comprise (a) a comparison, (b) the mean squared error, (c) regression analysis, (d) an error histogram, and (e) the ANN's training performance fit.

As demonstrated in Figure 6a, the ANN approach is applied separately from the AB method, which is used for numerically approximating the fractional-order differential equations. At epoch 413, the analyzed model achieves a mean squared error of $5.0769e-13$, as illustrated in Figure 6b. The training progression is displayed in Figure 6c, while the error histogram, highlighting the best result of $-6.2e-08$, is presented in Figure 6d. Figure 6e provides the optimal fit for training and testing datasets and their associated errors. The regression analysis for the model, encompassing all testing and training datasets, is shown in Figure 7. The results confirm that the model has been accurately trained, with data points aligning clearly along the regression line, yielding an R value close to 1.

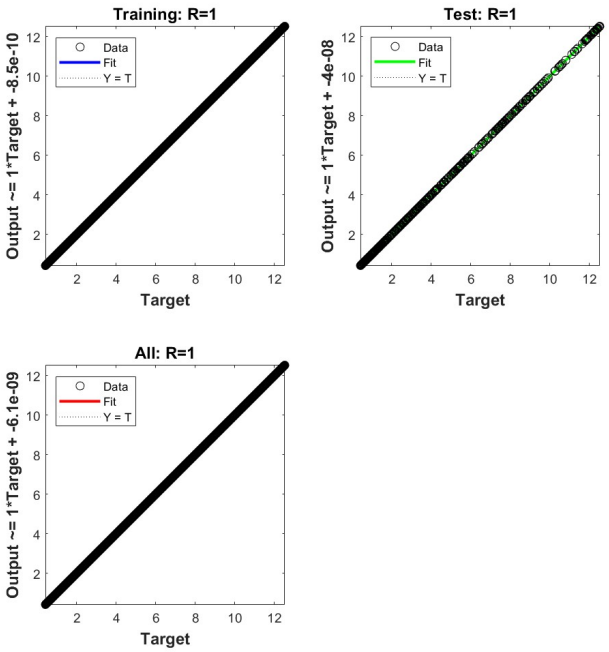

Figure 5. ANN-based regression was dynamically implemented to model the system's behavior being analyzed.

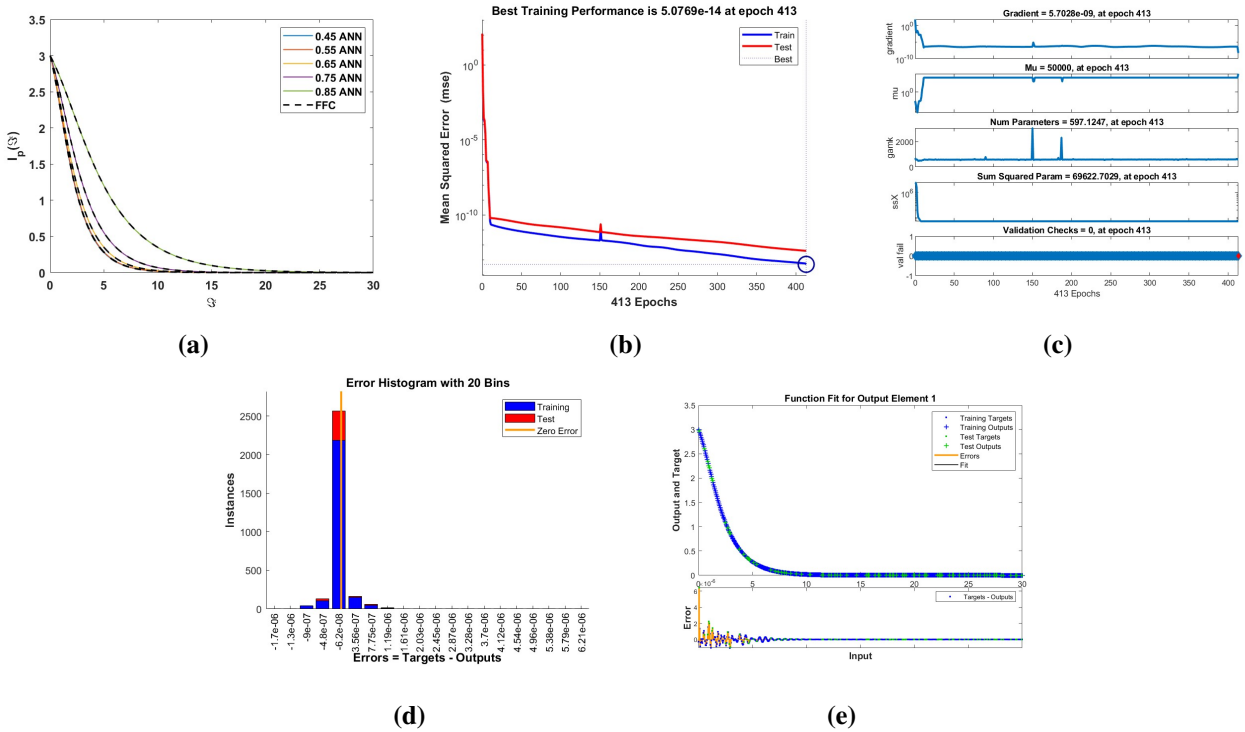

(a) **(b)** **(c)**

(d) **(e)**

Figure 6. The statistical dynamics of the analyzed model comprise (a) a comparison, (b) the mean squared error, (c) regression analysis, (d) an error histogram, and (e) the ANN's training performance fit.

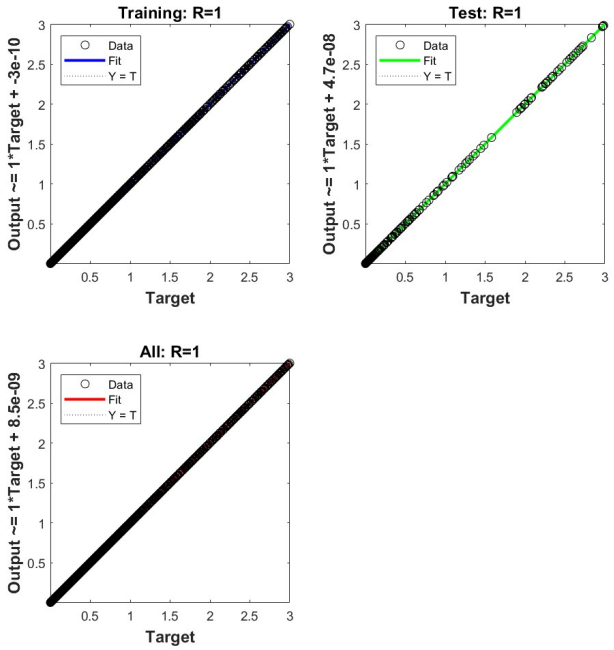

Figure 7. ANN-based regression was dynamically implemented to model the system's behavior being analyzed.

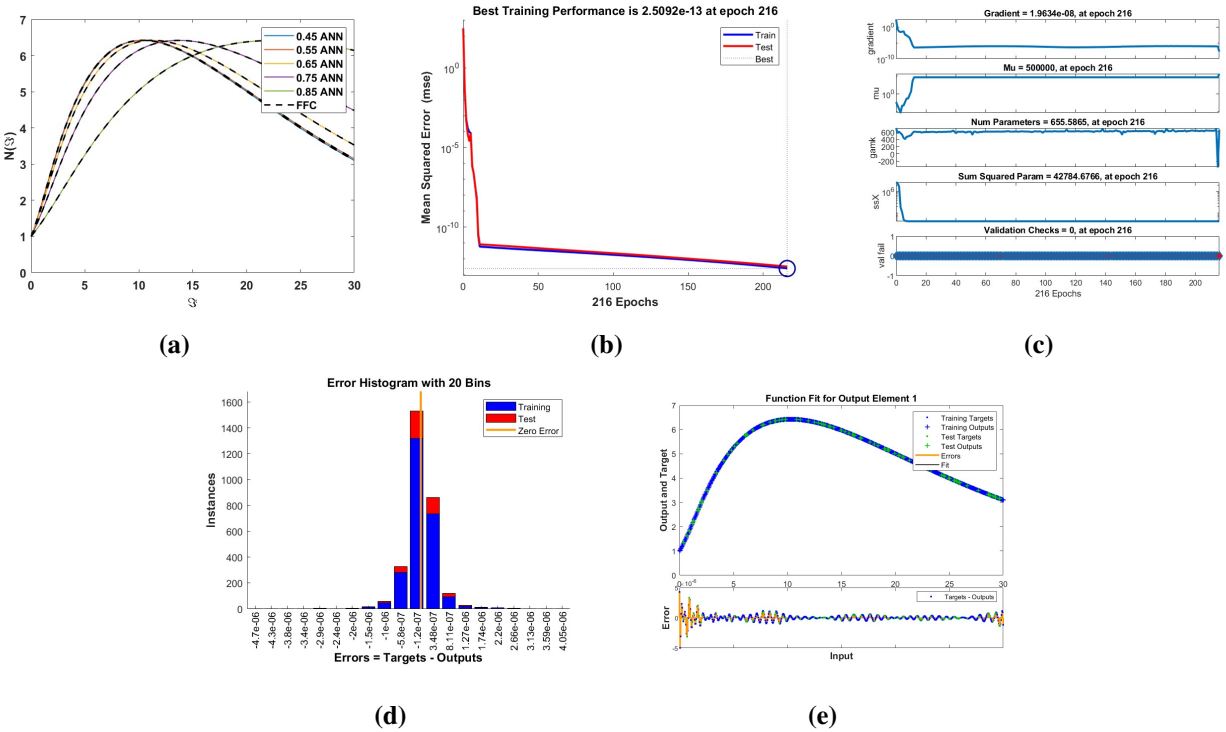

Figure 8. The statistical dynamics of the analyzed model comprise (a) a comparison, (b) the mean squared error, (c) regression analysis, (d) an error histogram, and (e) the ANN's training performance fit.

As depicted in Figure 8a, the ANN approach is implemented independently, while the AB method is used for the numerical approximation of fractional-order differential equations. At epoch 216, the model's performance achieves a mean squared error of $2.5092e-13$, as presented in Figure 8b. The training progression is illustrated in Figure 8c, while the error histogram, yielding the best result of $-1.2e-07$, is shown in Figure 8d. Figure 8e displays the optimal fit for training and testing datasets and their respective errors. Regression results for the complete dataset and training and testing subsets are shown in Figure 9. The results confirm the model's accurate training, with data points aligning closely along the regression line, resulting in an R value approximately equal to 1.

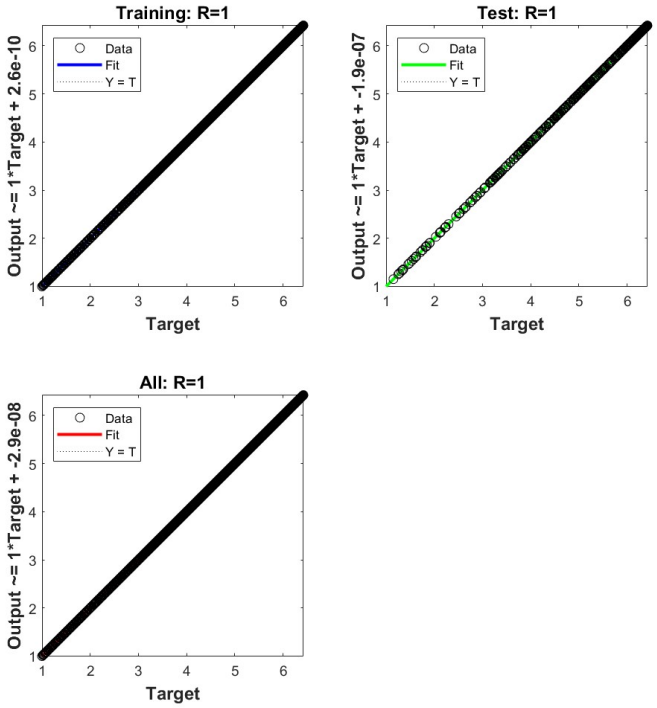

Figure 9. ANN-based regression was dynamically implemented to model the system's behavior being analyzed.

5. Conclusions

This study provides a comprehensive investigation into water quality management through a four-compartment fractional model incorporating the generalized ABC fractional operator. The compartmental dynamics are analyzed across different fractional orders, demonstrating the flexibility of varying the derivative order in modeling pollutant transport. The existence and uniqueness of solutions are established using the fixed-point approach, while UH stability methods confirm the model's stability. Additionally, approximate solutions are derived using the AB technique, ensuring computational efficiency. The study examines the effects of fractional orders and iterative intervals under diverse initial conditions, providing graphical comparisons against the integer-order case. The results indicate that lower fractional orders exhibit more stable behavior, whereas higher fractional

orders amplify pollutant transport dynamics, leading to prolonged contamination effects. Stability remains consistent at lower fractional orders but gradually diminishes as fractional order increases. Furthermore, integrating ANNs enables efficient dataset partitioning, facilitating training, testing, and validation while allowing for a comprehensive analysis of dataset characteristics and pollution trends. Compared to traditional integer-order models, the ABC fractional derivative provides a more accurate representation of memory effects in pollutant transport, making it highly effective for long-term contamination modeling. These findings emphasize the importance of fractional modeling in capturing persistent pollution dynamics, demonstrating its potential for enhancing real-world water quality management strategies.

Author contributions

Ateq Alsaadi: conceptualized and designed the study, conducted the investigation, prepared the original draft of the manuscript, validated the results, reviewed and edited the manuscript for clarity and accuracy, contributed to the development of the software tools used in the study, and secured funding; responsible for data curation, formal analysis, visualization, managed the project, overseeing research activities, and ensuring the timely completion of tasks. Author has read and approved the final version of the manuscript for publication.

Use of Generative-AI tools declaration

The author(s) declare(s) they have not used Artificial Intelligence (AI) tools in the creation of this article.

Acknowledgments

The authors extend their appreciation to Taif University, Saudi Arabia, for supporting this work through project number (TU-DSPP-2024-259).

Conflict of interest

The author declares no conflicts of interest in this paper.

References

1. R. P. Schwarzenbach, T. Egli, T. B. Hofstetter, U. Von Gunten, B. Wehrli, Global water pollution and human health, *Annu. Rev. Env. Resour.*, **35** (2010), 109–136. https://doi.org/10.1146/annurev-environ-100809-125342
2. J. I. Barzilay, W. G. Weinberg, J. W. Eley, The water we drink: Water quality and its effects on health, *Rutgers University Press*, 1999.
3. K. Rehman, F. Fatima, I. Waheed, M. S. H. Akash, Prevalence of exposure of heavy metals and their impact on health consequences, *J. Cell. Biochem.*, **119** (2018), 157–184. https://doi.org/10.1002/jcb.26234

4. D. Hinrichsen, S. Olsen Coastal waters of the world: Trends, threats, and strategies, *Island Press*, 1999.
5. G. Guo, G. Cheng, Mathematical modelling and application for simulation of water pollution accidents, *Process Saf. Environ.*, **127** (2019), 189–196. https://doi.org/10.1016/j.psep.2019.05.012
6. A. Issakhov, A. Alimbek, A. Abylkassymova, Numerical modeling of water pollution by products of chemical reactions from the activities of industrial facilities at variable and constant temperatures of the environment, *J. Contam. Hydrol.*, **252** (2023), 104116. https://doi.org/10.1016/j.jconhyd.2022.104116
7. I. Podlubny, *Fractional differential equations: An introduction to fractional derivatives, fractional differential equations, to methods of their solution and some of their applications*, 1998.
8. D. Baleanu, K. Diethelm, E. Scalas, J. J. Trujillo, *Fractional calculus: Models and numerical methods*, World Scientific, 2012.
9. M. Caputo, M. Fabrizio, A new definition of fractional derivative without singular kernel, *Progr. Fract. Differ. Appl.*, **1** (2015), 73–85.
10. L. Zhang, M. U. Rahman, S. Ahmad, M. B. Riaz, F. Jarad, Dynamics of fractional order delay model of coronavirus disease, *AIMS Mathematics*, **7** (2022), 4211–4232. https://doi.org/10.3934/math.2022234
11. M. Al-Refai, A. M. Jarrah, Fundamental results on weighted Caputo–Fabrizio fractional derivative, *Chaos Soliton. Fract.*, **126** (2019), 7–11. https://doi.org/10.1016/j.chaos.2019.05.035
12. M. Caputo, M. Fabrizio, Applications of new time and spatial fractional derivatives with exponential kernels, *Progr. Fract. Differ. Appl.*, **2** (2016), 1-11. https://doi.org/10.18576/pfda/020101
13. A. Atangana, D. Baleanu, New fractional derivatives with nonlocal and non-singular kernel: theory and application to heat transfer model, 2016, arXiv: 1602.03408. https://doi.org/10.48550/arXiv.1602.03408
14. W. Gao, B. Ghanbari, H. M. Baskonus, New numerical simulations for some real world problems with Atangana–Baleanu fractional derivative, *Chaos Soliton. Fract.*, **128** (2019), 34–43. https://doi.org/10.1016/j.chaos.2019.07.037
15. S. Qureshi, A. Yusuf, Modeling chickenpox disease with fractional derivatives: From caputo to atangana-baleanu, *Chaos Soliton. Fract.*, **122** (2019), 111–118. https://doi.org/10.1016/j.chaos.2019.03.020
16. A. Atangana, J. F. Gómez-Aguilar, Numerical approximation of Riemann-Liouville definition of fractional derivative: from Riemann-Liouville to Atangana-Baleanu, *Numer. Meth. Part. Differ. Equ.*, **34** (2018), 1502–1523. https://doi.org/10.1002/num.22195
17. M. ur Rahman, M. Yavuz, M. Arfan, A. Sami, Theoretical and numerical investigation of a modified ABC fractional operator for the spread of polio under the effect of vaccination, *AIMS Biophys.*, **11** (2024), 97–120. https://doi.org/10.3934/biophy.2024007
18. Z. Sabir, R. Sadat, M. R. Ali, S. B. Said, M. Azhar, A numerical performance of the novel fractional water pollution model through the Levenberg-Marquardt backpropagation method, *Arab. J. Chem.*, **16** (2023), 104493. https://doi.org/10.1016/j.arabjc.2022.104493

19. D. Baleanu, A. Jajarmi, S. S. Sajjadi, D. Mozyrska, A new fractional model and optimal control of a tumor-immune surveillance with non-singular derivative operator, *Chaos*, **29** (2019), 083127. https://doi.org/10.1063/1.5096159

20. P. Shekari, A. Jajarmi, L. Torkzadeh, K. Nouri, Fractional-order modeling of human behavior in infections: analysis using real data from Liberia, *Comput. Method. Biomec.*, 2025, 1–15. https://doi.org/10.1080/10255842.2024.2448559

21. R. Shafqat, A. Alsaadi, Artificial neural networks for stability analysis and simulation of delayed rabies spread models, *AIMS Mathematics*, **9** (2024), 33495–33531. https://doi.org/10.3934/math.20241599

22. A. Turab, R. Shafqat, S. Muhammad, M. Shuaib, M. F. Khan, M. Kamal, Predictive modeling of hepatitis B viral dynamics: A caputo derivative-based approach using artificial neural networks, *Sci. Rep.*, **42** (2024), 21853. http://doi.org/10.1038/s41598-024-70788-7

23. K. Abuasbeh, R. Shafqat, A. Alsinai, M. Awadalla, Analysis of the mathematical modelling of COVID-19 by using mild solution with delay Caputo operator, *Symmetry*, **15** (2023), 286. https://doi.org/10.3390/sym15020286

24. A. Ebrahimzadeh, A. Jajarmi, D. Baleanu, Enhancing water pollution management through a comprehensive fractional modeling framework and optimal control techniques, *J. Nonlinear Math. Phys.*, **31** (2024), 48. https://doi.org/10.1007/s44198-024-00215-y

25. B. Li, Z. Eskandari, Dynamical analysis of a discrete-time SIR epidemic model, *J. Franklin I.*, **360** (2023), 7989–8007. https://doi.org/10.1016/j.jfranklin.2023.06.006

26. M. El-Shebli, Y. Sharrab, D. Al-Fraihat, Prediction and modeling of water quality using deep neural networks, *Environ. Dev. Sustain.*, **26** (2024), 11397–11430. https://doi.org/10.1007/s10668-023-03335-5

27. E. Bonyaha, P. Agbekpornub, C. Unlud, Mathematical modeling of transmission of water pollution, *J. Prime Res. Math*, **17** (2021), 20–38.

28. A. Atangana, K. M. Owolabi, New numerical approach for fractional differential equations, *Math. Model. Nat. Phenom.*, **13** (2018), 3. https://doi.org/10.1051/mmnp/2018010

AIMS Press